

Unveiling Node Mass through Self-Consistent Gravity Model

Daekyung Lee^{1,2}, Wonguk Cho³, Heetae Kim¹, Gunn Kim^{4*}, Hyeong-Chai Jeong^{4,5} and Beom Jun Kim^{6*}

¹Department of Energy Engineering, Korea Institute of Energy Technology, Naju, 58322, Republic of Korea.

²Supply Chain Intelligence Institute Austria, Vienna, 1080, Austria.

³Graduate School of Data Science, Seoul National University, Seoul, 08826, Republic of Korea.

⁴Department of Physics and Astronomy & Institute for Fundamental Physics, Sejong University, Seoul, 05006, Republic of Korea.

⁵School of Computational Sciences, Korea Institute for Advanced Study, Seoul, 02455, Republic of Korea.

⁶Department of Physics, Sungkyunkwan University, Suwon, 16419, Republic of Korea.

*Corresponding author(s). E-mail(s): gunnkim@sejong.ac.kr; beomjun@skku.edu;

Abstract

The gravity model, inspired by Newton's law of universal gravitation, has long served as a primary tool for interpreting trade flows between countries, using a country's economic 'mass' as a key determinant. Despite its wide application, the definition of 'mass' within this model remains ambiguous. It is often approximated using indicators like GDP, which may not accurately reflect a country's true trade potential. Here, we introduce a data-driven, self-consistent numerical approach that redefines 'mass' from a static proxy to a dynamic attribute inferred directly from flow data. We infer mass distribution and interaction nature through our method, mirroring Newton's approach to understanding gravity. Our methodology accurately identifies predefined

embeddings and reconstructs system attributes when applied to synthetic flow data, demonstrating its strong predictive power and adaptability. Further application to real-world trade networks yields critical insights, revealing the spatial spectrum of trade flows and the economic mass of countries, two key features unexplored in depth by existing models. Our methodology not only enables accurate reconstruction of the original flow but also allows for a deep understanding of the unique capabilities of each node within the network. This study marks a significant shift in the understanding and application of the gravity model, providing a more comprehensive tool for analyzing complex systems and uncovering new insights into various fields, including global trade, traffic engineering, epidemic disease prevention, and infrastructure design.

Keywords: Gravity model, Inference algorithm, Data-driven analysis, Trade flow

1 Introduction

Natural phenomena have long served as sources of inspiration for theories to understand human behavior and social dynamics. Among these theories, the gravity model stands out, which draws an analogy between Newton's law of universal gravitation and the trade flow between countries[1, 2]. Essentially, this model posits that the trade volume between two countries is proportional to their economic 'mass' and inversely related to the distance between them. Over the past seventy years, this intuitive model has become a cornerstone of the study of international trade[3–9]. While early empirical applications were often criticized for their lack of theoretical basis, many theoretical advances have not only solidified its foundation[10–14] but also expanded its capacity to allow for a more consistent explanation of a broader range of phenomena[15–19].

However, one significant ambiguity remains in the gravity model. Given the absence of a method for measuring mass directly, most studies have used proxies, typically gross domestic product (GDP)[3–7]. This problem extends beyond trade studies; research in transportation[20–26], finance[27–31], and other social networks[32–36] also utilize external indicators to represent node attributes without rigorously evaluating their accuracy. This lack of a rigorous evaluation method impairs the fundamental consistency of the gravity model, consequently restricting its capacity to elucidate diverse human dynamics.

In the present work, we propose a *self-consistent* numerical method for the gravity model that significantly differs from traditional approaches. Unlike most conventional methods that rely on approximate proxies of mass, our method directly infers the mass and spatial dependency of the system based solely on the origin-destination flow data. This innovative approach not only improves the gravity model's consistency and precision but also transforms the role of mass from an external parameter into a distinctive metric for assessing

each entity's intrinsic capability to generate or attract flow. Our validation on a synthetic network reveals the method's remarkable ability to infer the predefined mass distribution and spatial dependencies, achieving near-perfect precision.

Furthermore, we apply our methodology to the international trade network data, analyzing the empirical characteristics of global trade. We confirm that our method more accurately infers the spatial dependency of the system and surpasses previous methods in reconstructing the original flow. Additionally, our economic mass metric enables the decoupling of each country's intrinsic trade capacity and the market effects of surrounding countries from total export/import data. This refined analysis enables us to analyze the detailed landscape of global trade, particularly emphasizing the significant influence of economic superpowers: the USA, China, and Germany. By advancing our understanding of the gravity model and its empirical application, our approach contributes to developing a perspective on the profound structure of global trade and has the potential to refine practices in related fields significantly.

2 Result

2.1 Previous approach and its limitation

In the conventional scheme of the gravity model, the directed flow f_{ij} from the i th to j th region is formulated as

$$f_{ij} = m_i^{\text{out}} m_j^{\text{in}} Q(d_{ij}), \quad (1)$$

where m_i^{out} and m_j^{in} denote the outward and inward *mass* of regions i , facilitating the initiation or attraction of flows. The $Q(d_{ij})$, known as the deterrence function, captures the effect of the distance d_{ij} between regions i and j on their interaction strength. It is important to note that the variables in this formulation fall into two categories: f_{ij} and d_{ij} are the measurable variables that can be obtained from the dataset, while m_i^{out} , m_i^{in} and $Q(d_{ij})$ are latent variables that describe the underlying landscape of the system. Consequently, the primary objective of the gravity model is to infer the values of m_i^{out} , m_i^{in} and $Q(d_{ij})$ based on available mobility or flow data $\{f_{ij}\}$ and the set of distances between nodes $\{d_{ij}\}$.

However, inferring the gravity model's latent variables is a notable challenge. Since the mass distribution and deterrence function reflect distinct aspects of flow data, simultaneous inference of both variables has been considered infeasible without additional information. As an alternative, many existing approaches approximate each node's mass with external variables and use them as a basis to calculate the system's spatial dependency. For instance, a country's GDP is frequently used to represent its mass in international trade networks[3, 4], and the population of a location is used as a similar indicator in transportation networks[20, 21, 37]. While those approaches offer some useful

insights and interpretations for certain areas, such assumptions pose questions about the consistency and validity of gravity model analysis.

To address these issues, L. S. Martyn suggested using each node’s total outward and inward flow as a measure of its mass in the corresponding direction[10]. In this “strength approximation”, node i ’s inward strength $S_i^{\text{in}} = \sum_j f_{ji}$ and outward strength $S_i^{\text{out}} = \sum_j f_{ij}$ are considered proportional to m_i^{in} and m_i^{out} , respectively. Despite its broad adoption in gravity model analyses, this approach has unveiled a significant issue regarding consistency in its theoretical foundation. According to the strength approximation, the bidirectional strength of node i can be expressed as

$$\begin{aligned} S_i^{\text{out}} &= \sum_j f_{ij} = m_i^{\text{out}} \sum_j A_{ij} m_j^{\text{in}} Q(d_{ij}) \propto S_i^{\text{out}} \sum_j A_{ij} S_j^{\text{in}} Q(d_{ij}) \\ S_j^{\text{in}} &= \sum_i f_{ij} = m_j^{\text{in}} \sum_i A_{ij} m_i^{\text{out}} Q(d_{ij}) \propto S_j^{\text{in}} \sum_i A_{ij} S_i^{\text{out}} Q(d_{ij}), \end{aligned} \quad (2)$$

where the superscripts “out” and “in” again correspond to each variable’s direction. A represents the adjacency matrix, and $A_{ij} = 1$ if there is a link between node i and node j , otherwise $A_{ij} = 0$. When contrasting the left and right sides of the equations, a clear inconsistency in scaling behavior emerges. For instance, if the $S_i^{\text{in,out}}$ in left side double, the right sides would quadruple. This scaling paradox reveals that strength cannot be a precise representation of mass but rather a fundamentally different variable. Despite efforts to rectify the discrepancies inherent in the strength approximation method, a conclusive resolution has yet to be achieved, leaving the precise depiction of mass an unresolved challenge. (We elucidate the details for the previous gravity model in Supplementary Section 1.)

2.2 Self-consistent inference formulation

In response to the challenges highlighted, we introduce a novel algorithm specifically designed for the gravity model inference. Our method accurately identifies the latent variable $\{m_i^{\text{out}}, m_i^{\text{in}}\}$, and $Q(d)$ through a fully self-consistent approach without the need for external data. The concept of our methodology is inspired by certain established techniques[10], previously developed for inferring one of two key variables when the other is available. Specifically, if the system’s mass distribution is obtained through an external proxy, these techniques can determine the deterrence function $Q(d)$, and *vice versa*. Although those techniques alone still necessitate external information, we have discovered that integrating these techniques creates a self-consistent loop where the mass and deterrence functions alternately refine each other. Beginning with simple initial conditions for the latent variables, our approach implements an iterative scheme that sequentially updates each component in alignment with the observed flow data $\{f_{ij}\}$. By directly deriving all latent variables without any external information, our method resolves the inherent

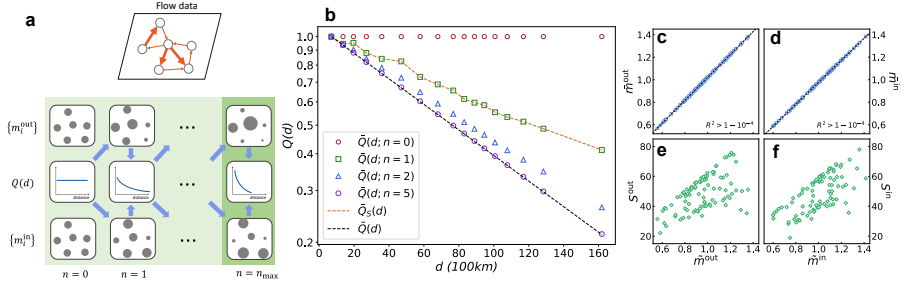


Fig. 1 The conceptual description of the self-consistent inference algorithm and its verification in model network. (a) The mass distribution $\{m_i^{\text{in, out}}\}$ and deterrence function $Q(d)$ are properly initialized in $n = 0$ and iteratively update each other to explain the flow dynamics of the system. (b) In the synthetic model network, the inference of deterrence function $\bar{Q}(d, n)$ quickly converges to the ground truth $\bar{Q}(d)$, while that of strength approximation $\bar{Q}_S(d)$ give a rather inaccurate result. [c - d] Comparison of synthetic input mass information $\{\bar{m}_i^{\text{out}}, \bar{m}_i^{\text{in}}\}$ and the inferred information $\{\bar{m}_i^{\text{out}}, \bar{m}_i^{\text{in}}\}$, respectively, from our self-consistent formulation of the gravity model. [e - f] Comparison of $\{\bar{m}_i^{\text{out}}, \bar{m}_i^{\text{in}}\}$ with the estimations from the simple strength approximation in which inward and outward mass distribution are approximated as $\{S_i^{\text{out}}, S_i^{\text{in}}\}$. Our self-consistent inference formulation can clearly reconstruct the information underlying synthetic data of f_{ij} while the strength-based simple gravity model fails.

dilemma faced by previous methods and achieves a significant advancement in the development of the gravity model.

The proposed formulation is graphically depicted in Fig. 1 (a). At the initial stage $n = 0$, the $\{m_i^{\text{out}}, m_i^{\text{in}}\}$ and $Q(d)$ are initialized as uniform distribution and constant function, which do not yet reflect the $\{f_{ij}\}$. Moving to stage $n = 1$, each node's mass is recalibrated based on the $Q(d)$ of the prior stage to represent its connected flows better; the nodes associated with larger outward flows in the actual data are assigned a greater outward mass, while those with significant inward flows are attributed a greater inward mass. Following this, the spatial dependency $Q(d)$ is updated based on the revised node mass distribution. Those iterative refinements enhance the model's alignment with actual flow dynamics $\{f_{ij}\}$ and continue until all inferred information converges to a stationary state. We explain the detailed procedure of our methodology in the method section.

2.3 Verification with synthetic data

In this section, we apply our inference formulation to flow data to evaluate its performance and conduct a comparative analysis with existing gravity model methodologies. Our objective is to assess whether this formulation can accurately identify the mass distribution and the deterrence function. Given the absence of known mass distribution and deterrence functions in real-world data, we turned to synthetic flow data generated based on mass and deterrence functions we assigned arbitrarily. If the outcomes from our algorithm align with those initial assumptions, it would indicate our method's effectiveness.

To commence, we specify arbitrary values for the mass distribution and deterrence function, denoted as $\{\tilde{m}_i^{\text{out}}, \tilde{m}_i^{\text{in}}\}$ and $\tilde{Q}(d)$. These variables enable us to compute the flow data $\{f_{ij}\}$, following Eq. (1). This generated data then acts as the input for our self-consistent formulation. Subsequently, we apply our inference technique to extract the inferred mass distribution $\bar{m}_i^{\text{out}}, \bar{m}_i^{\text{in}}$, and the inferred deterrence function $\bar{Q}(d)$. The accuracy of our methodology is determined by comparing these inferred quantities with the original variables, serving as our benchmark for success.

We use synthetic data based on an international trade network spanning 94 countries as a backbone structure. In this simulation, mass variable \tilde{m}_i^{out} and \tilde{m}_i^{in} are allocated randomly following a normal distribution with a mean of 1 and a standard deviation of 0.2. The deterrence function is assigned as $\tilde{Q}(d) = e^{-d/10000}$, representing one of its typical forms from previous research. The distance d_{ij} between a node pair is defined as the geodesic distance, in kilometers, between the reference location of the two countries measured along a great circle on the earth. We assign each country's reference location from countries.csv in Google Dataset Publishing Language[38]. With those latent and real variables, we calculate the flows f_{ij} according to Eq. (1), providing a benchmark for our model's performance.

Our gravity model initiates the inference process with a set of arbitrary initial values, iteratively updating mass distribution and deterrence function. This iterative cycle is continued until the inferred values— $\bar{m}_i^{\text{out}}, \bar{m}_i^{\text{in}}$, and $\bar{Q}(d)$ —no longer exhibit significant changes, indicating a steady state has been reached. It is important to note that these values include various scaling factors which need careful adjustment for accuracy. To ensure a fair comparison, we normalize the maximum value of the deterrence function to unity and adjust the averages of inward mass and outward mass distributions to be equal.

In Fig. 1 (b), we demonstrate the iterative refinement of inferred deterrence function $\bar{Q}(d; n)$, highlighting how it gradually aligns with the synthetic baseline $\tilde{Q}(d)$ over iterations $n = 1, 2$, and 5. Starting as a constant at $n = 0$, $\bar{Q}(d; n)$ undergoes adjustments at each step, marked distinctly for $n = 0, 1, 2, 5$. Despite limitations from piece-wise linear approximation and the binning process, by iteration $n = 5$, $\bar{Q}(d; n)$ aligns closely with $\tilde{Q}(d)$, depicted by the black dashed line representing our model's ground truth.

Furthermore, we compare this progression with the deterrence function $\bar{Q}^S(d)$ derived from the strength approximation, calculated as $\bar{Q}^S(d) = \langle f_{ij} / S_i^{\text{out}} S_j^{\text{in}} \rangle_{d \approx d_{ij}}$, applying the same binning strategy. Interestingly, after the first iteration, $\bar{Q}(d; n = 1)$ closely mirrors $\bar{Q}^S(d)$. We mark that this resemblance is attributed to the gravity model's intrinsic property. Specifically, under a constant $Q(d)$, the outward strength S_i^{out} —expressed as $\sum_j f_{ij} = m_i^{\text{out}} \sum_j A_{ij} m_j^{\text{in}} Q(d_{ij})$ —becomes proportional to m_i^{out} , since the summation across j is almost equivalent for all nodes i . This rationale similarly applies to the inward strength, making the deterrence function of the first iteration resemble $\bar{Q}^S(d)$. As we advance beyond the initial iteration, our model quickly diverges from these early parallels and converges towards $\bar{Q}(d)$, the synthetic

benchmark. This progression underscores our method’s capability to dynamically refine and accurately model the deterrence function within a synthetic network framework.

In Figs. 1 (c)-(f), we compare the synthetic input mass distribution $\tilde{m}_i^{\text{out}}, \tilde{m}_i^{\text{in}}$ with inferred values from our model and the strength approximation. Data points are arranged with the ground truth on the horizontal axis against the inferred masses and strengths on the vertical. Notably, in panels (c) and (d), the masses inferred by our model exhibit a tight correlation with the synthetic values, as demonstrated by a linear fit characterized by a high coefficient of determination. Conversely, the results from the strength approximation, depicted in panels (e) and (f), reveal a marked divergence from the synthetic benchmarks. This underscores the strength approximation’s limitations in accurately capturing the network’s intrinsic mass distribution.

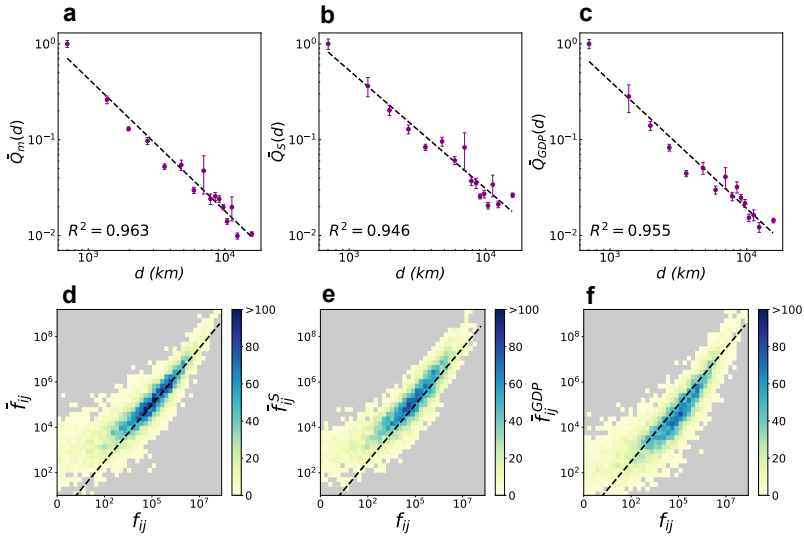


Fig. 2 [(a) - (c)] The deterrence functions $\bar{Q}_m(d)$, $\bar{Q}_S^S(d)$, and $\bar{Q}^{\text{GDP}}(d)$ for the 2019 international trade network, estimated using (a) our method, (b) the strength approximation, and (c) the GDP approximation, respectively. Although all functions follow a power-law decay pattern, the results from our method (a) feature narrower error bars and a more uniform decay pattern. [(d) - (f)] Density plots compare the actual trade flows, denoted by f_{ij} , with those predicted by the three methodologies. These include (d) our method with \hat{f}_{ij}^m , (e) the strength approximation with \hat{f}_{ij}^S , and (f) the GDP approximation with $\hat{f}_{ij}^{\text{GDP}}$. The plots visually underscore our method’s better ability to reconstruct the real flow data, particularly in regions of high trade flow.

2.4 International trade network analysis

This section aims to explore the practical applications of our gravity formulation by analyzing real-world data. Specifically, we use the international trade

network as our testbed, which closely aligns with the gravity model's primal topic. The 2019 international trade network data, sourced from the Trade Map of International Trade Center (ITC) [39], not only offers a comprehensive snapshot of global trade dynamics before the COVID-19 pandemic but also provides critical insights into the underlying mechanisms that drive the global economy [40]. In this network, each node i represents a country and a weighted directed edge f_{ij} denotes the total annual trade flow from country i to the country j , and their distance d_{ij} is again defined as the geodesic distance. Note that the ITC dataset includes over 100 countries. However, we use only the 94 countries included in all datasets for consistency with the other datasets introduced later. The list of these countries can be found in the supplement.

Employing our method, we estimate the mass distribution $\bar{m}_i^{\text{out}}, \bar{m}_i^{\text{in}}$ and the deterrence function $\bar{Q}(d)$, which stabilizes after five iterations ($n = 5$). We also use conventional strength and GDP-based approximations for a comparative analysis to estimate a country's mass. The GDP of each country is obtained from The World Bank database [41], and we include only countries with a GDP higher than 100 million dollars. We adjust each variable's scale to normalize the deterrence function's maximum to unity and to balance the mean values of the inward and outward mass distributions. In Fig. 2 (a)-(c), the derived deterrence functions are displayed: (a) $\bar{Q}_m(d)$ from our method, (b) $\bar{Q}^S(d)$ from the strength approximation, and (c) $\bar{Q}^{\text{GDP}}(d)$ from the GDP approximation. We also plotted the linear regression line in log space for each dataset, represented by the black dashed line. Our methodology results in smaller error bars and a higher coefficient of determination (R^2) for the linear regression line in (a), indicating superior accuracy and consistency compared to the alternative approximations.

As a further validation, We reconstruct the flow distribution $\{\bar{f}_{ij}\}$ by utilizing the inferred masses $\{\bar{m}_i^{\text{out}}, \bar{m}_i^{\text{in}}\}$ and the deterrence function $\bar{Q}(d)$ from various methods. To ensure consistency, we adjusted the scale of the reconstructed flow distribution to match the total flow sum of the actual data. The reconstruction is compared to the actual flow distribution $\{f_{ij}\}$, as illustrated in a density plot where the horizontal and vertical axes denote the actual and reconstructed flow, respectively. We draw a black dashed diagonal line in each plot, indicating perfect agreement. Our method's superiority is evident as it shows the highest density of points near the black dashed diagonal line. Also, we note that the goodness-of-fit measured by the Sørensen–Dice similarity index (SSI) is significantly higher for our method, as can be seen in Supplementary Fig. S3. Although our method slightly overestimates the flow values for smaller f_{ij} , it achieves significantly higher accuracy across most data points than strength and GDP-based approximations. This highlights the effectiveness of our method in capturing the dynamics of international trade flow. Taking into account the inevitability of incomplete data in real-world scenarios, we have also rigorously tested our method with the assumption of data incompleteness, demonstrating its robustness. This underscores the practical

utility of our approach for analyzing flow data within the international trade network, with further details provided in Supplementary Fig. S3.

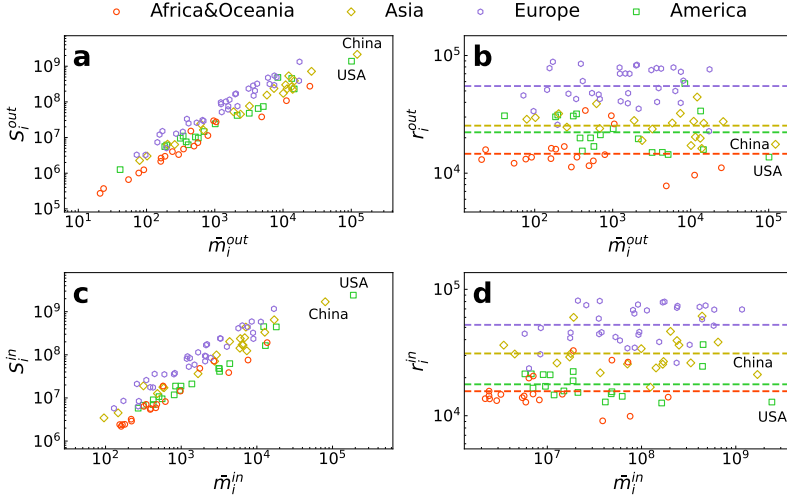


Fig. 3 Comparison of inferred mass and strength distribution for the international trade network. Symbols represent the country's mass and strength in each panel, classified by four continent labels. The left panels (a) and (c) illustrate the relationship between strength and mass, whereas the right panels (b) and (d) display the balance index, which represents the ratio of strength to mass for each node. The positioning of data points in the left panels is noticeably grouped according to their continent label, suggesting the geographical implication of the strength-mass ratio. The results in the right panels further emphasize these patterns in the balance index, with colored dashed lines indicating the geometric average of data points for each continent.

The inferred mass distributions at iteration $n = 5$ are illustrated in Fig. 3, and compared with the strength values using log-log scale scatter plots due to the data distribution (see Supplementary Fig. S1). This comparison is conducted separately for outward and inward quantities, presented in the top and bottom panels. Upon inspection, Fig. 3(a) exposes a prominent pattern: the majority of European countries (violet data points) exhibit a tendency toward relatively high bidirectional strength values, $S_i^{in,out}$, in relation to the corresponding outward mass inference values, $\bar{m}_i^{in,out}$. Conversely, most African and Oceanian countries (red data points) show the opposite trend. This pattern is consistent for both outward and inward quantities, as shown in Fig. 3(c).

We propose that the behaviors observed in Fig. 3 can be attributed to the inherent characteristics of the gravity model. Specifically, according to Eq.(1), the outward strength of node i is described as $S_i^{out} = \sum_j f_{ij} = \bar{m}_i^{out} \sum_j A_{ij} \bar{m}_j^{in} \bar{Q}(d_{ij})$. This formulation reveals that a node's outward strength is determined not solely by its own outward mass but also by the weighted sum of the inward masses of surrounding nodes. Consequently,

the ratio

$$r_i^{\text{out}} = \frac{S_i^{\text{out}}}{\bar{m}_i^{\text{out}}} = \sum_j A_{ij} \bar{m}_j^{\text{in}} \bar{Q}(d_{ij}) \quad (3)$$

serves as an indicator of external contribution to node i 's total exportation, which we term the External Advantage Index (EAI). Nodes encircled by others with substantial inward masses are likely to exhibit a high r_i^{out} , signifying a considerable export advantage due to their neighbors. Similarly, this logic applies to inward strength, S_i^{in} , which is expressed as the product of its inward mass and the weighted sum of surrounding nodes' outward mass, further illustrating the reciprocal nature of trade relationships.

This concept aligns with the observations from Fig. 3(a) and (c). European countries, characterized by their dense geographical distribution and substantial masses, tend to exhibit higher EAI values compared to the countries in Africa and Oceania. To further highlight the continent-specific characteristics of global trade, panels (b) and (d) plot the bidirectional EAI against the mass of each node, with colored lines representing the geometric average EAI for each continent. The geometric average is employed to precisely represent the tendency of data points distributed along log scale axes. The average EAI for European countries (violet) is notably highest, followed by those in Asia, America, Africa & Oceania, which are in decreasing order.

Country	S^{out}	m^{out}	S^{in}	m^{in}	r^{out}	r^{in}	$m^{\text{in}}/m^{\text{out}}$
USA	1382000	100900	2416000	188300	13.69	12.83	1.866
Germany	1331000	17460	1165000	16810	76.25	69.28	0.963
China	2150000	122200	1697000	80110	17.59	21.18	0.655

Table 1 Comparison of bidirectional mass and strength, and several applied quantities of three major countries: The USA, Germany, and China. We set the unit of strength and EAI as a billion dollar, and other quantities are unitless. The first four columns reveal that China and the USA have their advantage in exportation and importation, while those of Germany are relatively even. The next two columns exhibit the bidirectional EAI, and the last column denotes the ratio between inward and outward masses. All values in the table are presented with a precision of four significant figures.

Building on our findings about the mass and EAI distribution, we further explore the global trade landscape involving major economic powers. Given that a country's EAI is influenced by the economic mass of its neighbors, we hypothesize that the economic conditions of countries proximate to dominant trade powers are significantly shaped by these giants' economic scales. For instance, countries adjacent to major economic powers likely experience advantages in their import and export activities.

To analyze how these advantages manifest in detail, we examined the attributes of each country based on their proximity to dominant economic powers. Figure 4 displays each country's inward and outward EAI ($r_i^{\text{in},\text{out}}$) and their ratio ($R_i = r_i^{\text{out}}/r_i^{\text{in}}$) using a ternary plot. For geographic representation, each point on the plot is positioned according to deterrence functions with respect to three major economic powers: the USA, Germany, and China.

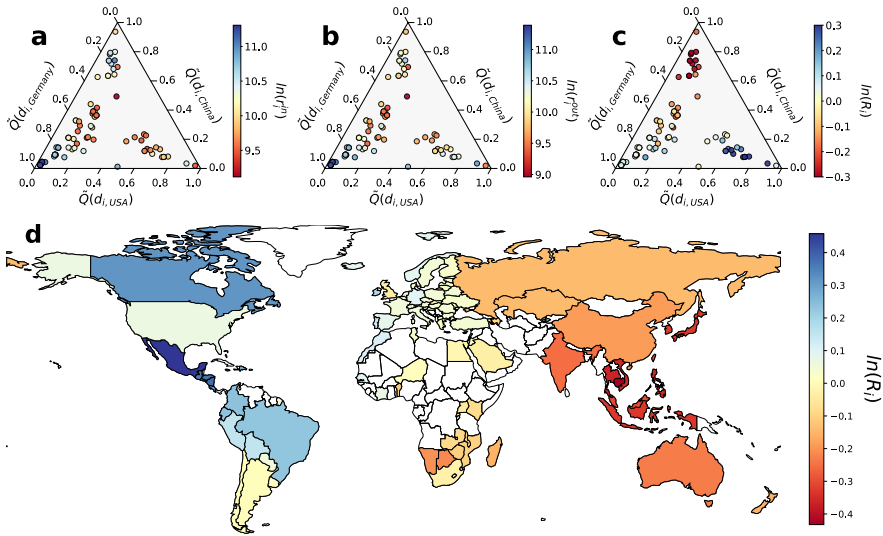


Fig. 4 The ternary plot illustrates the trade patterns of countries, arranged by their relative deterrance functions towards three major countries: Germany, the USA, and China. A logarithmic color scale is utilized to enhance the visualization of specific details. Panels (a) and (b) depict the External Advantage Index (EAI) for imports and exports, respectively. The analysis reveals that proximity to China and Germany correlates with advantages in importation and exportation, while proximity to the USA is mainly associated with export benefits. Panel (c) presents the Relative Advantage Index (RAI), defined as the ratio between outward and inward EAI, reflecting the economic characteristics of counties within the global trade network. This visualization effectively clusters data points according to the proximity of their closest major country. Furthermore, panel (d) illustrates the geographic distribution of RAI, providing insights into the spatial trade advantage landscape.

Consequently, each dominant country is denoted by a data point at its corresponding corner, and others are positioned based on proximity to these powers. We opted for log scale color mapping in all plots to illustrate the variable patterns effectively. The outcomes depicted in Figs. 4 (a) and (b) mostly concur with our hypotheses: the bidirectional EAI of each data point mainly increases as they approach the corners of plots due to each dominant country's substantial contribution to nearby countries' trade environment. (we also attached the geographic distribution of $r_i^{\text{in,out}}$ in Supplementary Fig. S2.)

In Fig. 4 (c), the ternary plot illustrates the out/in EAI ratio, which we term the Relative Advantage Index (RAI). It encapsulates the local economic context of country i regarding its trade balance, highlighting the relative advantage of a country's exports over its imports. In this plot, pronounced clustering is evident, with each data point closely aligning with the economic influence of its nearest major country. Specifically, countries close to the USA and China show marked advantages in exports and imports, respectively, while those near Germany display balanced advantages in both sectors. This pattern of relative trade advantages is further emphasized in Fig. 4 (d), which

displays the geographic distribution of RAI and reveals distinct segregation among countries in the global trade landscape.

To elucidate the observed tendency, we analytically assess the influence of dominant countries on their neighbors. Specifically, for a given country i , when a dominant country p exhibits substantially higher $\bar{m}_p^{\text{in},\text{out}}$ and $Q(d_{ip})$ values compared to i 's other neighbors, we express the RAI relative to the dominant country's metrics as

$$R_i = \frac{r_i^{\text{out}}}{r_i^{\text{in}}} = \frac{\sum_j A_{ij} \bar{m}_j^{\text{in}} \bar{Q}(d_{ij})}{\sum_j A_{ji} \bar{m}_j^{\text{out}} \bar{Q}(d_{ji})} \approx \frac{\bar{m}_p^{\text{in}}}{\bar{m}_p^{\text{out}}}. \quad (4)$$

This equation shows that a country's RAI (R_i) is heavily influenced by the trade characteristics of its dominant neighbor. Specifically, if the neighbor primarily focuses on exports, the surrounding countries are likely to see increased benefits from imports. Conversely, if the neighbor is mainly import-oriented, it may boost export opportunities for these countries. In other words, the dominant countries' intrinsic economic characteristics significantly influence neighboring countries' trade environments, further shaping the landscape of the global trade network.

The pronounced clustering behavior of the R_i distribution in Fig. 4 (c) strongly supports our interpretation, with each data point's value closely aligning with the inward-to-outward mass ratio of its nearest dominant country: $\frac{m_{\text{USA}}^{\text{in}}}{m_{\text{USA}}^{\text{out}}} > 1$, $\frac{m_{\text{Germany}}^{\text{in}}}{m_{\text{Germany}}^{\text{out}}} \approx 1$, and $\frac{m_{\text{China}}^{\text{in}}}{m_{\text{China}}^{\text{out}}} < 1$ as detailed in Table. 1. The geographic distribution of R_i , as depicted in Fig. 4 (d), further corroborates this clustering behavior, underscoring the significant influence of these major economies.

Building on these insights, we can infer that the geographical landscape of international trade is profoundly shaped by the economic characteristics of these three major countries. The United States' import-centric economy affects the export conditions of its neighboring countries. In contrast, China's export-oriented economy allows its nearby countries to enhance their total importation. Similarly, Germany's relatively balanced economy enables neighboring countries to optimize their trade capabilities in both sectors.

3 Discussion

We have developed a self-consistent inference formulation for gravity models that transcends the fundamental limitations inherent in previous approaches. Our method uniquely circumvents the need for external proxies or approximations by directly utilizing flow and distance data, enabling the simultaneous deduction of mass distribution and the deterrence function. Starting with basic assumptions about mass and deterrence, our iterative refinement process relies solely on the inherent data, eliminating the need for supplementary external data.

Our novel framework not only enables the extraction of significant model parameters directly from raw data but also significantly improves the model's

accuracy and scope of application. Through numerical simulations with synthetic datasets, we have demonstrated that our approach outperforms conventional gravity model methods, such as strength approximation, in identifying the ground truth of mass and deterrence function.

The application of our model to actual international trade networks has provided profound insights into the global trade landscape. By comparing each country's inferred mass and total export/import, our framework successfully decouples its total trade volume into intrinsic capability and external influences. In particular, our findings indicate that the strength-to-mass ratios capture the country's local economic advantage, which is related to the neighboring countries' mass distributions and proximity.

Furthermore, our analysis has unveiled that the economic advantages of individual countries are significantly influenced by the economic characteristics of dominant countries such as the United States, Germany, and China within their vicinity. We found that countries located near these economic superpowers, characterized by either export- or import-oriented economic structures, derive notable benefits in terms of their own exports or imports. This observation allows us to reinterpret the landscape of the global trade network, highlighting how it is shaped around these dominant countries.

Our formulation introduces a novel metric for assessing the intrinsic trade capabilities of counties, paving the way for diverse and promising avenues of further development and exploration. For instance, analyzing the temporal evolution of global mass distribution could shed light on the nuanced dynamics of economic phenomena. Additionally, examining the spatial distribution of mass within mobility networks could unveil the complex landscape of transport networks. Beyond these, our method holds potential for applications and expansions for supply chain network, social networks, ecological dynamics, and numerous other research fields, significantly broadening their investigative horizons.

In conclusion, our study introduces an innovative self-consistent inference formulation for gravity models, enhancing the methodology beyond the limitation of traditional approaches. This advancement refines the paradigm of gravity modeling, reducing the dependency on external data and enabling a more direct exploration of the phenomena within the gravity model framework. The development and application of our approach shed light on new avenues for analyzing complex phenomena. Future research has the opportunity to build on this foundation, further enriching the gravity model's application in various contexts.

4 Method

4.1 Algorithm Detail and Implementation

Our numerical algorithm procedure consists of successive stages. In the initial stage of the simulation (at step $n = 0$), we establish a baseline where both the outward and inward masses for each node i are set to unity ($\bar{m}_i^{\text{out}}(0) =$

$\bar{m}_i^{\text{in}}(0) = 1$), and the deterrence function $\bar{Q}(d; 0)$ is uniformly initialized to 1 for all distance values d . This initialization serves as a neutral foundation for the iterative dynamics that follow.

During each iteration step, we adjust the mass distributions to explain the flow data based on the spatial dynamics observed up to the previous step n , employing two key update formulas:

$$\bar{m}_i^{\text{out}}(n+1) = \frac{S_i^{\text{out}}}{\sum_j A_{ij} \bar{m}_j^{\text{in}}(n) \bar{Q}(d_{ij}; n)}, \quad (5)$$

where S_i^{out} represents the total outward flow from node i . The inward mass, $\bar{m}_j^{\text{in}}(n+1)$, for node j follows a similar updating scheme:

$$\bar{m}_j^{\text{in}}(n+1) = \frac{S_j^{\text{in}}}{\sum_i A_{ij} \bar{m}_i^{\text{out}}(n) \bar{Q}(d_{ij}; n)}, \quad (6)$$

with S_j^{in} encapsulating the total inward flow to node j . Note that those update processes match the strength of each node with the respective generated strength.

Each iteration includes a critical update to the deterrence function, $\bar{Q}(d_k; n+1)$, reflecting changes in node interactions and spatial relationships at step $n+1$. R. Cazabet also mentioned a similar concept in his work [42] and suggested an iterative update of the deterrence function, without detailed analysis. This update uses a piece-wise linear approximation based on equal-frequency binning, which divides the range of distances into segments containing equal numbers of node pairs to ensure uniform sampling across varied distances. This binning technique sorts the distance data, $\{d_{ij}\}$, and groups them into predefined bins, each containing an equal number of data points. If the total number of data points is not divisible by the bin size, the last bin is adjusted to include the remainder, ensuring that it contains slightly more data points as necessary. Within each bin, the deterrence function's value, $\bar{Q}(d_k; n+1)$, is updated based on the average of node pairs that fall within the bin's distance range. Specifically, the update formula is given by:

$$\bar{Q}(d_k; n+1) = \frac{1}{N_k} \sum_{(i,j) \in \text{bin } k} \frac{f_{ij}}{\bar{m}_i^{\text{out}}(n+1) \bar{m}_j^{\text{in}}(n+1)}, \quad (7)$$

where N_k denotes the number of node pairs within each bin k . This methodical approach to updating the deterrence function ensures that the model accurately reflects the underlying spatial and interaction dynamics of the network, facilitating a robust simulation of the system's evolution over time.

Since these updates do not inherently constrain the scales of the variables, we establish their scales through specific criteria. First, we adjust all f_{ij} by a constant factor to ensure that the total inferred flow matches the total real flow. The deterrence function $\bar{Q}(d)$ is normalized such that its maximum value is 1. Finally, we adjust the remaining scales by ensuring that the average of all \bar{m}_i^{out} equals the average of all \bar{m}_j^{in} .

4.2 Data availability

The authors declare that the data supporting the findings of this study are available within the paper and its supplementary information files. The filtered dataset used in the analysis is available from the corresponding authors upon reasonable request.

Supplementary information. This file contains supplementary text, supplementary figures 1 – 3, supplementary equations 1 – 3, and supplementary references.

Acknowledgments. B. J. Kim acknowledges support from the National Research Foundation of Korea (NRF) grant funded by the Korean government (MSIT) (Grant No. 2019R1A2C2089463). D. Lee and H. Kim acknowledge support from the NRF grant funded by the Korean government (MSIT) (Grant No. NRF-2022R1C1C1005856). H. C. Jeong acknowledge support from the NRF grant funded by the Korean government (MSIT) (Grant No. NRF-2021R1F1A1063238).

Declarations

Competing Interests. The authors declare no competing interests.

Contributions. D.L., G.K., H.-C.J., and B.J.K. conceived the research and developed the methodology. W.C. extracted the data. D.L. performed the simulations, and all authors analyzed the results. D.L., B.J.K., and W.C. wrote the manuscript under the supervision of all other authors.

References

- [1] Tinbergen, J.: Shaping the World Economy: Suggestions for an International Economic Policy. Twentieth Century Fund study. Twentieth Century Fund, New York (1962)
- [2] Anderson, J.E.: The gravity model. *Annu. Rev. Econ.* **3**, 133–160 (2011). <https://doi.org/10.1146/annurev-economics-111809-125114>
- [3] Mishra, A.K., Gadhia, J.N., Kubendran, N., Sahoo, M.: Trade flows between india and other brics countries: An empirical analysis using gravity model. *Glob. Bus. Rev.* **16**(1), 107–122 (2015). <https://doi.org/10.1177/0972150914553523>
- [4] Cheng, I.-H., Wall, H.J.: Controlling for heterogeneity in gravity models of trade and integration. *Fed. Reserve Bank St. Louis Rev.* **87**, 49–63 (2005)
- [5] Helpman, E., Melitz, M.J., Rubinstein, Y.: Estimating trade flows: Trading partners and trading volumes. *Q. J. Econ.* **123**(2), 441–487 (2008)

- [6] Eaton, J., Kortum, S.: Technology, geography, and trade. *Econometrica* **70**(5), 1741–1779 (2002)
- [7] Head, K., Mayer, T.: Gravity equations: Workhorse, toolkit, and cookbook. *Handb. Int. Econ.* **4**, 131–195 (2014)
- [8] Santos Silva, J.M.C., Teneyro, S.: The log of gravity. *Rev. Econ. Stat.* **88**(4), 641–658 (2006)
- [9] Bergstrand, J.H.: The gravity equation in international trade: Some microeconomic foundations and empirical evidence. *Rev. Econ. Stat.* **67**(3), 474–481 (1985)
- [10] Senior, M.L.: From gravity modelling to entropy maximizing: a pedagogic guide. *Prog. Hum. Geogr.* **3**(2), 175–210 (1979). <https://doi.org/10.1177/030913257900300218>
- [11] Evans, A.W.: Some properties of trip distribution methods. *Transp. Res.* **4**(1), 19–36 (1970). [https://doi.org/10.1016/0041-1647\(70\)90072-9](https://doi.org/10.1016/0041-1647(70)90072-9)
- [12] Anderson, J.E., van Wincoop, E.: Gravity with gravitas: A solution to the border puzzle. *Am. Econ. Rev.* **93**(1), 170–192 (2003)
- [13] Baldwin, R., Taglioni, D.: Gravity for dummies and dummies for gravity equations. NBER Work. Pap. (12516) (2006)
- [14] Deardorff, A.V.: Determinants of bilateral trade: Does gravity work in a neoclassical world? *Natl. Bur. Econ. Res.* **5377**, 7–32 (1998)
- [15] Stewart, J.Q.: Demographic gravitation: Evidence and applications. *Sociometry* **11**(1/2), 31–58 (1948)
- [16] Pan, R.K., Kaski, K., Fortunato, S.: World citation and collaboration networks: uncovering the role of geography in science. *Sci. Rep.* **2**(1), 902 (2012). <https://doi.org/10.1038/srep00902>
- [17] Li, X., Tian, H., Lai, D., Zhang, Z.: Validation of the gravity model in predicting the global spread of influenza. *Int. J. Environ. Res. Public Health* **8**(8), 3134–3143 (2011)
- [18] Cevik, S.: Going viral: A gravity model of infectious diseases and tourism flows. *Open Econ. Rev.* (2021)
- [19] Simini, F., González, M.C., Maritan, A., Barabási, A.-L.: A universal model for mobility and migration patterns. *Nature* **484**(7392), 96–100 (2012)

- [20] Jung, W.-S., Wang, F., Stanley, H.E.: Gravity model in the korean highway. *EPL* **81**(4), 48005 (2008). <https://doi.org/10.1209/0295-5075/81/48005>
- [21] Hong, I., Jung, W.-S.: Application of gravity model on the korean urban bus network. *Physica A* **462**, 48–55 (2016). <https://doi.org/10.1016/j.physa.2016.06.055>
- [22] Krings, G., Calabrese, F., Ratti, C., Blondel, V.D.: Urban gravity: a model for inter-city telecommunication flows. *J. Stat. Mech.: Theory Exp.* **2009**(07), 07003 (2009). <https://doi.org/10.1088/1742-5468/2009/07/L07003>
- [23] Liang, X., Zhao, J., Dong, L., Xu, K.: Unraveling the origin of exponential law in intra-urban human mobility. *Sci. Rep.* **3**(1), 2983 (2013). <https://doi.org/10.1038/srep02983>
- [24] Kwon, O., Jung, W.-S.: Intercity express bus flow in korea and its network analysis. *Physica A* **391**(17), 4261–4265 (2012). <https://doi.org/10.1016/j.physa.2012.03.031>
- [25] Li, R., Gao, S., Luo, A., Yao, Q., Chen, B., Shang, F., Jiang, R., Stanley, H.E.: Gravity model in dockless bike-sharing systems within cities. *Phys. Rev. E* **103**, 012312 (2021). <https://doi.org/10.1103/PhysRevE.103.012312>
- [26] Song, J., Abuduwayiti, A., Gou, Z.: The role of subway network in urban spatial structure optimization – wuhan city as an example. *Tunn Undergr Space* **131**, 104842 (2023). <https://doi.org/10.1016/j.tust.2022.104842>
- [27] Portes, R., Rey, H.: The determinants of cross-border equity flows. *J. Int. Econ.* **65**(2), 269–296 (2005)
- [28] Lane, P.R., Milesi-Ferretti, G.M.: International investment patterns. *Rev. Econ. Stat.* **90**(3), 538–549 (2008)
- [29] Fidora, M., Fratzscher, M., Thimann, C.: Home bias in global bond and equity markets: The role of real exchange rate volatility. *J. Int. Money Financ.* **26**(4), 631–655 (2007)
- [30] Coeurdacier, N., Martin, P.: The geography of asset trade and the euro: Insiders and outsiders. *J. Int. Econ.* **77**(2), 195–210 (2009)
- [31] Hellmanzik, C., Schmitz, M.: Taking gravity online: The role of virtual proximity in international finance. *J. Int. Money Finance* **77**, 164–179 (2017). <https://doi.org/10.1016/j.jimonfin.2017.07.001>

- [32] Mazur, L., Suesse, T., Krivitsky, P.N.: Investigating foreign portfolio investment holdings: Gravity model with social network analysis. *Int. J. Financ. Econ.* **27**(1), 554–570 (2022). <https://onlinelibrary.wiley.com/doi/pdf/10.1002/ijfe.2168>. <https://doi.org/10.1002/ijfe.2168>
- [33] Jin, P.J., Cebelak, M., Yang, F., Zhang, J., Walton, C.M., Ran, B.: Location-based social networking data: Exploration into use of doubly constrained gravity model for origin–destination estimation. *Transp. Res. Rec.* **2430**(1), 72–82 (2014). <https://doi.org/10.3141/2430-08>
- [34] Li, Z., Ren, T., Ma, X., Zhang, P., Yang, Z., Ding, Y.: Identifying influential spreaders by gravity model. *Sci. Rep.* **9**(1), 8387 (2019)
- [35] Singh, H., Singh, H.: An enhanced gravity model for determining crucial nodes in social networks based on degree k-shell eigenvector index. *IEEE Access* **12**, 23163–23180 (2024). <https://doi.org/10.1109/ACCESS.2024.3363635>
- [36] Li, S., Xiao, F.: The identification of crucial spreaders in complex networks by effective gravity model. *Inf. Sci.* **578**, 725–749 (2021). <https://doi.org/10.1016/j.ins.2021.08.026>
- [37] Sun, Q., Wang, S., Zhang, K., Ma, F., Guo, X., Li, T.: Spatial pattern of urban system based on gravity model and whole network analysis in eight urban agglomerations of china. *Math. Probl. Eng.* **2019**, 6509726 (2019)
- [38] Google: Dataset Publishing Language: countries.csv. <https://github.com/google/dspl/blob/master/samples/google/canonical/countries.csv>
- [39] International Trade Center: Trade Map - Trade statistics for international business development. <https://www.trademap.org/>
- [40] Cho, W., Lee, D., Kim, B.J.: A multiresolution framework for the analysis of community structure in international trade networks. *Sci. Rep.* **13**(1), 5721 (2023)
- [41] Bank, W.: World Development Indicators. <https://databank.worldbank.org/source/world-development-indicators>
- [42] Cazabet, R., Borgnat, P., Jensen, P.: Enhancing space-aware community detection using degree constrained spatial null model. In: Gonçalves, B., Menezes, R., Sinatra, R., Zlatić, V. (eds.) *Complex Networks VIII*, pp. 47–55. Springer, Cham (2017)